

THE STRIKINGLY SIMILAR RELATION BETWEEN SATELLITE AND CENTRAL GALAXIES AND THEIR DARK MATTER HALOS SINCE $z = 2$

DOUGLAS F. WATSON^{1,2} AND CHARLIE CONROY³

Draft version August 16, 2018

ABSTRACT

Satellite galaxies in rich clusters are subject to numerous physical processes that can significantly influence their evolution. However, the typical L^* satellite galaxy resides in much lower mass galaxy groups, where the processes capable of altering their evolution are generally weaker and have had less time to operate. To investigate the extent to which satellite and central galaxy evolution differs, we separately model the stellar mass - halo mass ($M_* - M_h$) relation for these two populations over the redshift interval $0 < z < 1$. This relation for central galaxies is constrained by the galaxy stellar mass function while the relation for satellite galaxies is constrained against recent measurements of the galaxy two-point correlation function (2PCF). Our approach does not rely on the abundance matching technique but instead adopts a flexible functional form for the relation between satellite galaxy stellar mass and subhalo mass, where subhalo mass is considered at the maximum mass that a subhalo has ever reached in its merger history, M_{peak} . At $z \sim 0$ the satellites, on average, have $\sim 10\%$ larger stellar masses at fixed M_{peak} compared to central galaxies of the same halo mass (although the two relations are consistent at $2 - 3\sigma$ for $M_{\text{peak}} \gtrsim 10^{13} M_\odot$). This is required in order to reproduce the observed stellar mass-dependent 2PCF and satellite fractions. At low masses our model slightly under-predicts the correlation function at ~ 1 Mpc scales. At $z \sim 1$ the satellite and central galaxy $M_* - M_h$ relations are consistent within the errors, and the model provides an excellent fit to the clustering data. At present, the errors on the clustering data at $z \sim 2$ are too large to constrain the satellite model. A simple model in which satellite and central galaxies share the same $M_* - M_h$ relation is able to reproduce the extant $z \sim 2$ clustering data. We speculate that the striking similarity between the satellite and central galaxy $M_* - M_h$ relations since $z \sim 2$ arises because the central galaxy relation evolves very weakly with time and because the stellar mass of the typical satellite galaxy has not changed significantly since it was accreted. The reason for this last point is not yet entirely clear, but it is likely related to the fact that the typical $\sim L^*$ satellite galaxy resides in a poor group where transformation processes are weak and lifetimes are short.

Subject headings: cosmology: theory — dark matter — galaxies: halos — galaxies: evolution — galaxies: formation — large-scale structure of universe

1. INTRODUCTION

Understanding the evolution of stellar mass in galaxies is a crucial piece in the galaxy formation puzzle. Substantial effort has been devoted to constraining how the stellar content of galaxies is related to their dark matter halos, which provides a fundamental bridge between observation and theory. Such stellar mass - halo mass relations ($M_* - M_h$) have yielded a variety of novel insights, including constraints on the efficiency of galaxy formation and connections between galaxy growth and halo growth over much of cosmic time (White et al. 2007; Zheng et al. 2007; Conroy & Wechsler 2009; Yang et al. 2012; Moster et al. 2013; Behroozi et al. 2012a,b; Leitner 2012; Wang et al. 2012). There is a growing consensus that the $M_* - M_h$ relation evolves little over most of cosmic history; the implications of this non-evolution are only beginning to be explored.

Galaxies can be classified as ‘central’ or ‘satellite’ de-

pending on whether they are located near the center of a parent dark matter halo or whether they reside within a larger system. Satellite galaxies can lead tumultuous lives as they orbit within the intense gravitational field of their host halo (e.g., Kravtsov et al. 2004b). A number of complex processes can therefore affect the stellar mass evolution of satellite galaxies, including: (1) cold gas stripping due to ram pressure (Gunn & Gott 1972), (2) ‘strangulation’ (Larson et al. 1980), which removes the hot gas reservoir surrounding satellites, thereby reducing the fuel available to feed the cold gas disk on long timescales, (3) shredding of satellite galaxies due to tidal stripping (Purcell et al. 2007; Watson et al. 2012), and (4) gravitational interactions with other nearby galaxies known as ‘harassment’ (Moore et al. 1998). These effects leave observational signatures on features such as galaxy star formation histories, colors, morphologies, and the amount and spatial distribution of intrahalo light. While much attention has focused on the evolution of satellites in clusters, where these effects tend to be maximally important, the typical $\sim L^*$ satellite galaxy resides in poor groups (Zehavi et al. 2005; van den Bosch et al. 2007; Zehavi et al. 2011). It may therefore be the case that the evolution of the typical satellite galaxy is not markedly different from the average central galaxy, at

¹ NSF Astronomy & Astrophysics Postdoctoral Fellow, Department of Astronomy & Astrophysics, The University of Chicago, Chicago, IL 60637, USA

² Kavli Institute for Cosmological Physics, 5640 South Ellis Avenue, The University of Chicago, Chicago, IL 60637, USA

³ Department of Astronomy & Astrophysics, University of California, Santa Cruz, CA, 95064, USA

the same stellar mass. Understanding the relation between satellite galaxies and their dark matter subhalos (self-bound, dark matter structures orbiting in the potential of their host halo), and how this relation differs from the relation between central galaxies and their parent halos, has the potential to constrain the importance of these various complex physical processes, and is the primary goal of the present work.

There are two general approaches to constraining the $M_* - M_h$ relation. First, there is the halo occupation distribution (HOD) technique (and the closely related conditional luminosity function technique Yang et al. 2003), which adopts flexible functional forms for mapping galaxies into dark matter halos (e.g., Peacock & Smith 2000; Seljak 2000; Scoccimarro et al. 2001; Berlind & Weinberg 2002; Cooray & Sheth 2002; Zheng et al. 2007; Leauthaud et al. 2012). Conceptually, galaxies are separated into centrals and satellites, with the centrals residing at rest at the center of a parent dark matter halo. Satellites are then modeled as orbiting within parent dark matter halos, with some additional assumptions regarding their radial and velocity profiles. This approach does not explicitly use any information about dark matter subhalos (i.e., satellites are not constrained to reside within subhalos). The second technique is known as abundance matching (Kravtsov et al. 2004a; Vale & Ostriker 2004; Tasitsiomi et al. 2004; Vale & Ostriker 2006; Conroy et al. 2006; Conroy & Wechsler 2009; Guo et al. 2010; Simha et al. 2010; Neistein et al. 2011b; Watson et al. 2012; Reddick et al. 2012; Rodríguez-Puebla et al. 2012; Hearin et al. 2012). In this approach galaxies are assigned to dark matter halos such that galaxy and halo mass are monotonically related with the most massive galaxies residing in the most massive halos. In this case subhalos are used to place satellite galaxies in the cosmic web. The abundance matching technique requires as an input the spatial abundance of objects, i.e., the luminosity or mass function of galaxies. Despite its simplicity, this technique has been shown to reproduce a variety of observations including galaxy two-point correlation functions (2PCFs) (Conroy et al. 2006; Reddick et al. 2012), close pair counts (Berrier et al. 2006; Berrier & Cooke 2012), $M_* - M_h$ relations (Conroy & Wechsler 2009; Wang & Jing 2010; Guo et al. 2010; Reddick et al. 2012), and group multiplicity functions (Hearin et al. 2012). However, several studies have noted discrepancies between abundance matching predictions and galaxy statistics at low- z (e.g., Hearin et al. 2012) and intermediate redshifts (e.g., Wetzel & White 2010; Gerke et al. 2012), and we expound on these shortcomings in more detail throughout the paper. Recently, Behroozi et al. (2012b, hereafter B12) constrained $M_* - M_h$ relations over most of cosmic history using a different technique, where satellites were placed in dark matter subhalos, and in which the $M_* - M_h$ relation was flexibly parameterized and fit to a suite of data rather than being derived directly via the abundance matching formalism (a technique first introduced by Moster et al. 2010).

A key assumption made in most modeling efforts that place satellites in dark matter subhalos is that the satellite galaxy – subhalo mass relation is identical to the central galaxy – halo mass relation (with the appropriate

choice for the subhalo mass; see Section 2). In the present work we relax this assumption and attempt to separately constrain the satellite $M_* - M_h$ relation using galaxy clustering measurements and, where available, directly estimated satellite fractions. This approach has also been taken recently by Wang et al. (2006), Neistein et al. (2011a), and Rodríguez-Puebla et al. (2012). Such an approach can help address a variety of questions about satellite galaxies. For instance, *How well does the stellar mass- halo mass relation of satellite galaxies trace the central galaxy relation? How does the satellite relation evolve with redshift? Is there strong evolution in the peak and characteristic mass scale for satellite galaxy star formation efficiency?*

The rest of this paper is organized as follows. In § 2 we discuss the simulation and halo catalogs used in this study. In § 3 we lay out our theoretical framework, in § 4 we present our results, and a discussion is presented in § 5. Finally, in § 6 we give a summary of our work. Throughout we assume a Chabrier (2003) IMF and a flat Λ CDM cosmological model with $\Omega_m = 0.27$ and $\Omega_\Lambda = 0.73$. Regarding the Hubble constant, we assume $H_0 = 70 \text{ km s}^{-1} \text{ Mpc}^{-1}$ throughout, except when comparing to $z \sim 0$ clustering and satellite fraction data where we assume the convention of those data: $H_0 = 100 h \text{ km s}^{-1} \text{ Mpc}^{-1}$.

2. SIMULATION AND HALO CATALOGS

In the present work we employ the Bolshoi high resolution collisionless N -body simulation of cold dark matter (Klypin et al. 2011). The simulation has a volume of $250 h^{-3} \text{ Mpc}^3$ with 2048³ particles and a standard cold dark matter (Λ CDM) cosmological model with $\Omega_m = 0.27$, $\Omega_\Lambda = 0.73$, $\Omega_b = 0.042$, $h = 0.7$, $\sigma_8 = 0.82$, and $n_s = 0.95$. The simulation has a mass resolution of $1.9 \times 10^8 M_\odot$ and force resolution of $1 h^{-1} \text{ kpc}$, and particles were tracked from $z = 80$ to $z = 0$. Bolshoi was run with the Adaptive Refinement Tree Code (ART; Kravtsov et al. 1997; Kravtsov & Klypin 1999).

Halos and subhalos were identified with the phase-space temporal halo finder ROCKSTAR (Behroozi et al. 2011a,b). ROCKSTAR is capable of resolving the maximum circular velocity, $v_{\text{max}} \equiv \sqrt{GM(< r)/r}|_{\text{max}}$, of halos and subhalos down to a minimum value of $\sim 55 \text{ km s}^{-1}$. We use the ROCKSTAR halo catalogs at $z = 0.05, 0.9$ and 1.9 to model the satellite galaxy $M_* - M_h$ relation for clustering measurements at these same (median) redshifts. Halo masses were calculated using spherical overdensities according to the redshift-dependent virial overdensity formalism of Bryan & Norman (1998). Halo centers are defined as being located at the peak in the phase-space density distribution (see § 3.5.1 of Behroozi et al. 2011b for details).

Throughout this work we consider the halo mass definition M_{peak} for subhalos, which is the maximum mass that a subhalo has ever reached in its merger history. As we discuss in § 3, our theoretical framework is built off the $M_* - M_h$ relation of B12 which employs M_{peak} , thus we adopt this definition for consistency. M_{peak} is closely related to the commonly used M_{acc} , the mass of a subhalo at the epoch of accretion⁴. These quan-

⁴ We have repeated our analysis using subhalos at M_{acc} and find our results to be consistent with those based on M_{peak} .

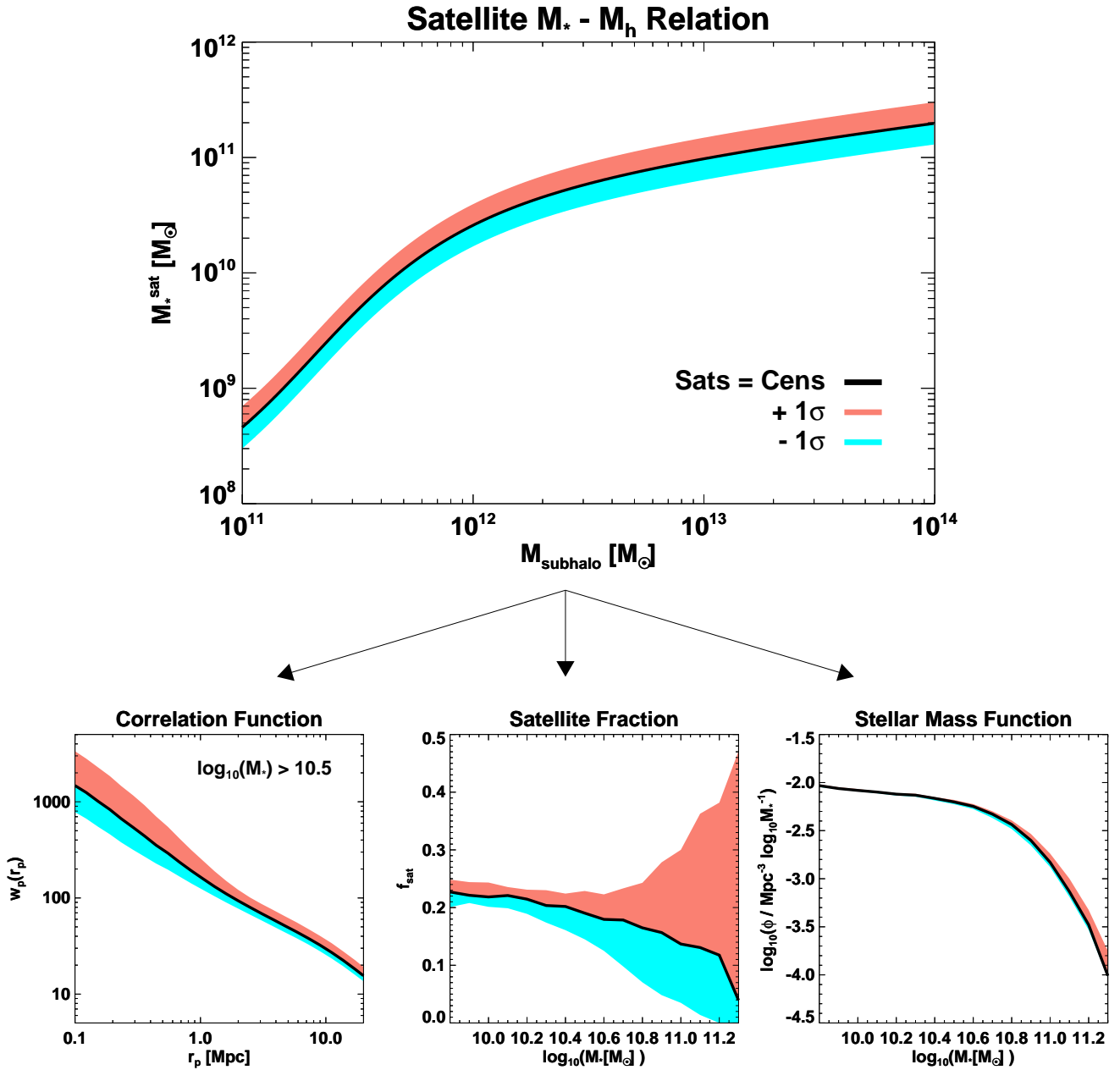


Figure 1. “Proof of concept” demonstrating the effect of varying the satellite galaxy $M_* - M_h$ relation on the two-point correlation function, satellite fraction, and stellar mass function. The top panel shows the satellite stellar mass - halo mass relation at $z \sim 0$, where the solid black curve is the *Sats=Cens* model of Behroozi et al. (2012b), such that the satellite $M_* - M_h$ relation is fixed to the central galaxy relation. The solid red and blue bands show the 1σ deviation associated with this relation (~ 0.2 dex scatter). By populating a high-resolution N-body simulation with stellar masses based on this mapping, we compute the projected galaxy two-point correlation function for a mass threshold $\log(M_*) > 10.5 M_{\odot}$ (bottom left panel), the satellite fraction (bottom middle panel), and the galaxy stellar mass function (bottom right panel). Both the satellite fraction and the correlation function are very sensitive to variation in the satellite $M_* - M_h$ relation. In contrast, the stellar mass function is hardly affected by the $\pm 1\sigma$ shift in the satellite $M_* - M_h$ relation because satellite galaxies are a minority population. This allows us to alter the satellite relation in order to match clustering measurements and satellite fractions (where available) while still ensuring that the model reproduces the global stellar mass function.

ities are important because subhalos lose mass due to tidal stripping throughout their orbital history. However, the galaxy is typically much more centrally concentrated than the halo, and so it is expected to undergo tidal stripping only after its halo has been nearly destroyed. Thus we expect the galaxy content of a subhalo to be more closely tied to the mass of the halo at the epoch of accretion or its maximum mass throughout its history, rather than the present mass of the halo (see e.g., Nagai & Kravtsov 2005; Vale & Ostriker 2006; Conroy et al. 2006; Reddick et al. 2012, for further discussion on this point).

3. THEORETICAL FRAMEWORK

Our approach begins with the $M_* - M_h$ relation of B12, which was constrained to match observational measurements of galaxy stellar mass functions (GSMFs), star formation rate-stellar mass relations, and the cosmic star formation history over the redshift range $0 < z < 8$. We retain the B12 relation for central galaxies, since the low- z observed satellite fractions imply that one-point statistics like the GSMF are primarily sensitive to central galaxies. In our approach the satellite $M_* - M_h$ relation is constrained by observed 2PCF data and, where available, direct estimates of the satellite fraction from group catalogs.

B12 chose a $M_* - M_h$ form that was flexible enough to reproduce the highly constraining low- z measurements, but not so flexible as to allow for over-fitting of data at higher redshifts where the uncertainties can be large. The specific functional form is given as:

$$\log_{10}(M_*(M_h)) = \log_{10}(\epsilon M_1) + f\left(\log_{10}\left(\frac{M_*}{M_h}\right)\right) - f(0), \quad (1)$$

where

$$f(x) = -\log_{10}(10^{\alpha x} + 1) + \delta \frac{(\log_{10}(1 + \exp(x)))^\gamma}{(1 + \exp(10^{-x}))}.$$

The virial mass at the epoch of observation is used for the halo mass of central galaxies, while M_{peak} is used for subhalos which harbor the satellites. The 5 parameters governing the fitting function are⁵: (1) the characteristic halo mass M_1 , (2) the ratio of the characteristic stellar and halo masses $\epsilon = M_0^*/M_1$, (3) the low-mass slope α , (4) the index of the subpower law⁶ of the $M_* - M_h$ relation high-mass slope γ , and (5) the strength of the subpowerlaw at the massive end δ . There is also scatter in the $M_* - M_h$ relation, ξ , which is assumed to be a log-normal distribution and constant with (sub)halo mass. We will call the model where satellites and centrals are given the same $M_* - M_h$ relation as determined in B12, the *Sats=Cens* model. The model in which the satellite $M_* - M_h$ relation is allowed to differ from the central relation will be called the *varySats* model.

⁵ Commonly used $M_* - M_h$ relations have a double power-law form with 4 principal parameters describing a characteristic halo/stellar mass and low/high-mass power slopes. B12 demonstrated that this double power-law formalism can not accurately match GSMFs at various redshifts (see Appendix D of B12).

⁶ A subpower law is a function that is asymptotically shallower than any power law, yet asymptotically greater than a logarithm.

The ‘‘proof of concept’’ of our technique is shown in Figure 1. The top panel shows the mean satellite galaxy $M_* - M_h$ relation at $z \sim 0$ for the best-fit *Sats=Cens* model of B12, with the solid red and blue bands depicting the 1σ deviation (~ 0.2 dex scatter in the $M_* - M_h$ relation). We populate the halos and subhalos from the Bolshoi simulation with stellar masses based on the *Sats=Cens* prescription and compute the projected 2PCF (bottom left panel), the satellite fraction (bottom middle panel), and the GSMF (bottom right panel). The details of the modeling are discussed below. The crucial point is how the 1σ error propagates into these three statistics. The 2PCF and the satellite fraction ($f_{\text{sat}} = n_{\text{sat}}/n_{\text{tot}}$) are very sensitive to the satellite $M_* - M_h$ relation. For the 2PCF this is especially notable on scales $r_p \lesssim 1$ Mpc (we are showing a mass threshold $\log(M^*) > 10.5 M_\odot$ as this corresponds to a mass cut used by Reddick et al. (2012) that we compare to throughout the paper). One can think of the 2PCF as a sum of two terms: on small scales, pairs of galaxies reside in the same host dark matter halo (the ‘1-halo’ term), whereas on large scales, the individual galaxies of a pair reside in distinct halos (the ‘2-halo’ term). The shape and amplitude of the 2PCF on small scales ($r \lesssim 1$ Mpc) are thus very sensitive to central-satellite and satellite-satellite pairs. f_{sat} is sensitive to changes in the satellite $M_* - M_h$ relation at all galaxy stellar masses, though the effect is most marked at the high-mass end. However, notice that the GSMF is hardly affected at all by the $\pm 1\sigma$ shift in the satellite $M_* - M_h$ relation since satellite galaxies are subdominant by number. The fraction of galaxies that are satellites at low redshift reaches a maximum value of $f_{\text{sat}} \sim 30\%$ for luminosity-selected samples (e.g., Zheng et al. 2005; Zehavi et al. 2011) and decreases with increasing redshift (Zheng et al. 2007; Wake et al. 2011). Therefore, we have some freedom to adjust the satellite $M_* - M_h$ relation to match clustering measurements while still remaining within the observational uncertainties of the global GSMF.

We take the following procedure to constrain the satellite $M_* - M_h$ relation:

1. Adopt the $M_* - M_h$ relation for the central galaxies derived in B12. Parametrize the normalization of the central relation via the following prefactor⁷:

$$\log_{10}(\epsilon_{\text{cen}}) = c_0 \times \log_{10}(\epsilon) \quad (2)$$

2. Parametrize the satellite relation such that subhalos are labeled according to their peak mass, M_{peak} , and pre-factors have been inserted in front of all the B12 $M_* - M_h$ relation parameters (as well as the scatter) such that,

$$\begin{aligned} \log_{10}(M_{1,\text{sat}}) &= c_1 \times \log_{10}(M_1) \\ \log_{10}(\epsilon_{\text{sat}}) &= c_2 \times \log_{10}(\epsilon) \end{aligned}$$

⁷ In principle, one would opt to insert pre-factors in front of all of the parameters associated with the B12 central $M_* - M_h$ relation. We have found this to be too computationally expensive to put into practice.

$$\begin{aligned}
\alpha_{\text{sat}} &= c_3 \times \alpha \\
\gamma_{\text{sat}} &= c_4 \times \gamma \\
\delta_{\text{sat}} &= c_5 \times \delta \\
\xi_{\text{sat}} &= c_6 \times \xi.
\end{aligned}
\tag{3}$$

3. Start with the *Sats=Cens* model parameter values (i.e., $c_{i=1\dots6} = 1.0$) and populate the halos and subhalos of the Bolshoi simulation with stellar masses based on this $M_* - M_h$ relation.
4. Compute the real-space two-point correlation function from the simulation for a given stellar mass threshold sample. For comparison to data, convert either to the projected, $w_p(r_p)$, or angular correlation function, $w(\theta)$. The former is computed via:

$$w_p(r_p) = 2 \int_0^{\pi_{\text{max}}} \xi\left(\sqrt{r_p^2 + \pi^2}\right) d\pi, \tag{4}$$

with the same upper limit of integration as used in the observational samples. The angular correlation function is computed using the Limber transformation,

$$w(\theta) = \frac{2}{c} \int_0^\infty dz H(z) N(z)^2 \int_0^\infty \xi(\sqrt{u^2 + D_m(\bar{z})^2 \theta^2}) du, \tag{5}$$

where c is the speed of light, $H(z)$ is the Hubble constant at redshift z , $N(z)$ is the normalized redshift distribution of the galaxies in the sample, and $D_m(\bar{z})$ is the comoving distance to the median redshift.

5. Compute the likelihood between the observed and predicted clustering for all available stellar mass threshold samples. Do this separately, not simultaneously, for the three redshifts considered: $z \sim 0, 1$ and 2 . Incorporate the measured satellite fraction as an additional constraint where available⁸.
6. Use a Markov Chain Monte Carlo (MCMC) method, varying the parameters $c_{i=0-6}$, to compute the range of possible satellite $M_* - M_h$ relations given the data. Specifically, adopt the Metropolis-Hastings algorithm, which works as follows. With the initial free parameter values from step 3, compute χ^2 from this starting point. Steps are then chosen for the parameters and χ^2 is computed for the new location. This new location is added to the chain if $\chi_{\text{new}}^2 < \chi_{\text{old}}^2$ or $n < \exp[-(\chi_{\text{new}}^2 - \chi_{\text{old}}^2)/2]$, where n is a random number between 0 and 1. If these conditions are not met, then the old location is repeated in the chain.

⁸ Direct estimates of satellite fractions are not available at $z \sim 1$ and 2 and so this additional constraint is not considered at those epochs. It is also true that $w_p(r_p)$ and f_{sat} are highly covariant. We do not take this into account in our modeling, though this should be incorporated in future work.

This process then repeats until the chain has converged⁹.

In the present work we focus on the satellite $M_* - M_h$ relation at $z \sim 0, 1$, and 2 . At $z \sim 0$ we consider a recent measurement of the stellar mass-dependent 2PCF derived by Reddick et al. (2012) using the New York University Value Added Galaxy Catalog (Blanton et al. 2005), based on the Sloan Digital Sky Survey (SDSS) Data Release 7 (Padmanabhan et al. 2008; Abazajian et al. 2009). We also use satellite fractions derived in Reddick et al. from SDSS group catalogs. The group catalogs were constructed according to the methodology described in Tinker et al. (2013). At $z \sim 1$ we employ two-point clustering measurements from the DEEP2 Galaxy Redshift Survey (Newman et al. 2012) by Mostek et al. (2012, hereafter M12). At $z \sim 2$ constraints are provided by angular clustering measurements from the NEWFIRM Medium Band Survey (NMBS; van Dokkum et al. 2009) as derived in Wake et al. (2011). In the following section we confront our model with these data.

4. RESULTS

We now compare the *Sats=Cens* and *varySats* models to observational constraints at $z \sim 0$ and 1 , and the *Sats=Cens* model to data at $z \sim 2$. We derive satellite $M_* - M_h$ relations at $0 < z < 1$ and investigate its evolution and how it compares to that of central galaxies. We also present satellite fractions over the interval $0 < z < 2$.

4.1. Clustering and the Satellite $M_* - M_h$ Relation at $z \sim 0$

Figure 2 shows the projected 2PCF at $z \sim 0$ at three separate stellar mass thresholds: $\log(M^*) > 10.1, 10.5$, and $11.1 M_\odot$. The black dashed curves show the *Sats=Cens* model where the clustering is computed from the best-fit $M_* - M_h$ relation given by B12. We emphasize that this curve is *not* a fit to the clustering data, rather it is a direct prediction of the B12 $M_* - M_h$ relation. The *Sats=Cens* model provides an excellent fit to the data at the largest stellar mass thresholds and on large scales, but under-predicts the clustering on small scales in the two lower mass samples.

This under-prediction is probably not due to resolution effects in the Bolshoi simulation, as discussed in Appendix B of Reddick et al. (2012). In addition, Watson et al. (2012) used the Zentner et al. (2005) semi-analytic model for subhalos, which has the capability of tracking subhalos down to circular velocities $\sim 0 \text{ km s}^{-1}$, to test resolution effects in numerical simulations. They performed a test in which they selected a $v_{\text{max}}^{\text{acc}} > 210 \text{ km s}^{-1}$ threshold (corresponding to $\sim L^*$ galaxies and brighter) with two additional v_{max} thresholds of $v_{\text{max}} > 20 \text{ km s}^{-1}$ and $v_{\text{max}} > 80 \text{ km s}^{-1}$ to

⁹ We incorporate the full covariance matrices for our model fitting at $z \sim 0$ and 2 . Covariance matrices are not available for the DEEP2 $z \sim 1$ samples. We assume non-informative, uniform priors on the parameters and we start numerous chains at a wide range of initial c pre-factor values to confirm that they converge to the same parameter values. For more details on MCMC techniques, see Dunkley et al. (2005).

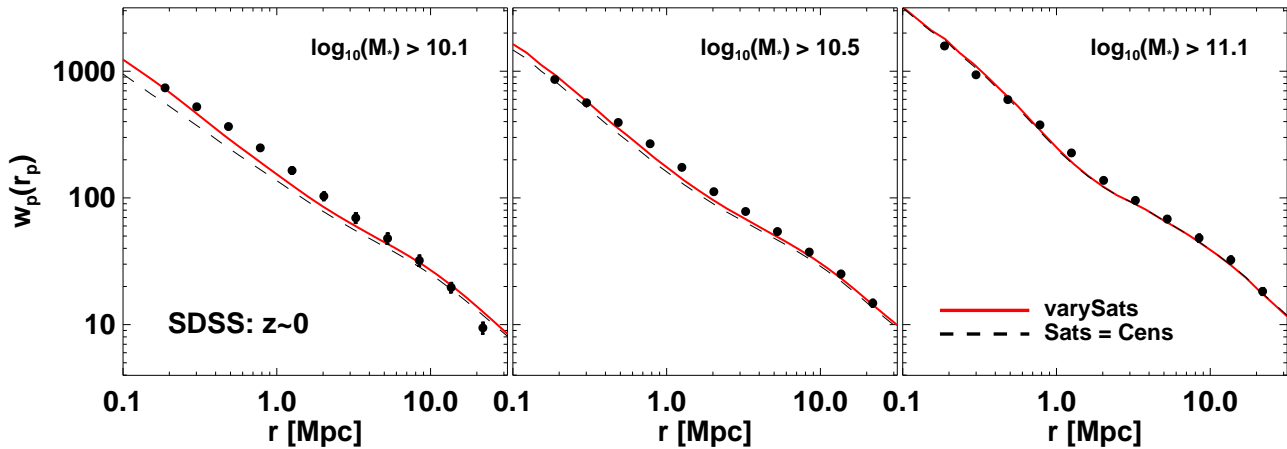


Figure 2. Comparison between model and observed projected correlation function as a function of stellar mass for three SDSS threshold samples as measured by Reddick et al. (2012): $\log(M^*) > 10.1, 10.5, 11.1 M_\odot$. The black dashed curve shows the *Sats=Cens* model prediction where the satellite $M_* - M_h$ relation is fixed to that of the central galaxies. The red solid curve shows our best-fit model in which the $M_* - M_h$ relation for satellite galaxies is allowed to vary to better match observed clustering and satellite fractions (see Figure 3). There is still tension between the *varySats* model and the data at the 1-2 halo transition, especially at lower masses.

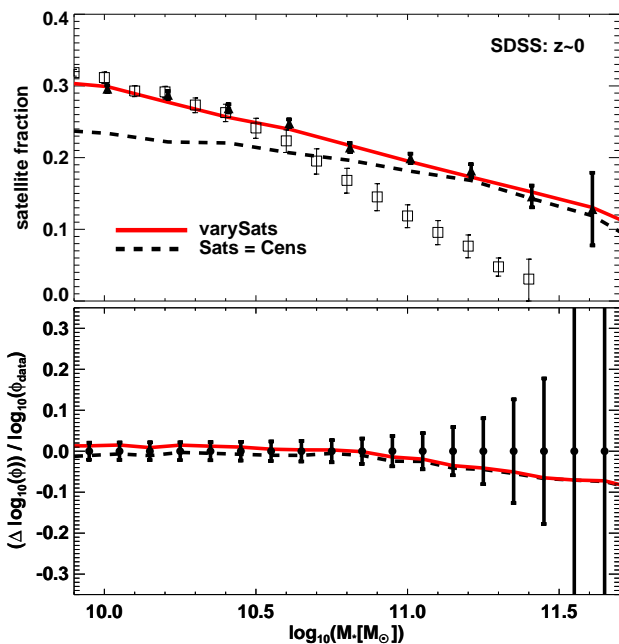


Figure 3. *Top panel:* Best-fit model satellite fraction (red curve) as a function of galaxy stellar mass (black data points with error bars are from Reddick et al. 2012). The *Sats=Cens* model clearly fails to reproduce the measured satellite fractions at low masses, while the *varySats* model is in good agreement with the data. We also show the satellite fractions as measured by Yang et al. (2009) as open black boxes and in the text we discuss the implications of the discrepancy at $\log(M_*) \gtrsim 10.7$ on our modeling results. *Bottom panel:* Residuals between the observed and model galaxy stellar mass function; data are from Baldry et al. (2008). The galaxy stellar mass function is dominated by central galaxies, so varying the satellite galaxy $M_* - M_h$ relation has little effect on the galaxy stellar mass function and is within the errors.

mimic the effect of a resolution limit of a given simulation. Increasing this threshold from 20 to 80 km s^{-1} resulted in a maximum $\sim 20\%$ decrease in the 2PCF

at scales $r \lesssim 1$ Mpc. Increasing from 20 to 40 km s^{-1} only had a few percent effect on the small-scale amplitude. Though not explicitly shown in their paper, they repeated this test for $v_{\text{max}}^{\text{acc}} > 170 \text{ km s}^{-1}$ and found nearly the same result, implying that the resolution limit of 55 km s^{-1} should not have a significant effect on the 2PCF for the lowest stellar mass threshold considered in Figure 2.

We have also constructed 1000 *Sats=Cens* models drawing from the errors in the B12 best-fit parameters and found the 1σ distribution in the 1000 2PCFs to still be significantly discrepant from the data on small scales at lower masses. Thus, no *Sats=Cens* model can provide a satisfactory fit to the small-scale clustering for the lowest stellar mass threshold sample.

The *Sats=Cens* model succeeds on large scales because the large-scale clustering is only weakly sensitive to the treatment of satellite galaxies. On smaller scales the 2PCF is much more sensitive to the relation between satellite galaxy mass and halo mass. The *varySats* model allows for freedom in the satellite $M_* - M_h$ relation and thus is able to more closely match the data shown in Figure 2, though there is clearly still unresolved tension at the 1- and 2-halo junction at ~ 1 Mpc.

In addition to the 2PCF, the *varySats* model is also constrained by the measured satellite fraction, shown in Figure 3. As we see in the top panel of Figure 3, the data require a larger satellite fraction for $\log(M^*) < 10.9 M_\odot$ than the prediction of the *Sats=Cens* model. The open squares are the measurements of Yang et al. (2009) for comparison to the R12 results. We use R12 throughout the paper for consistency with the simulation and data used in B12. However, group-finder effects can lead to large biases at large M_* and the Yang et al. (2009) data are clearly discrepant with R12 at $\log(M_*) \gtrsim 10.7$. Specifically, this arises because R12 does not assume that central galaxies are necessarily the most massive (or brightest) in their host halo (see § 7.3 of R12 for details). The disagreement becomes relevant at very large stellar masses, $\log(M_*) \gtrsim 10.7$. Thus, this may affect our mod-

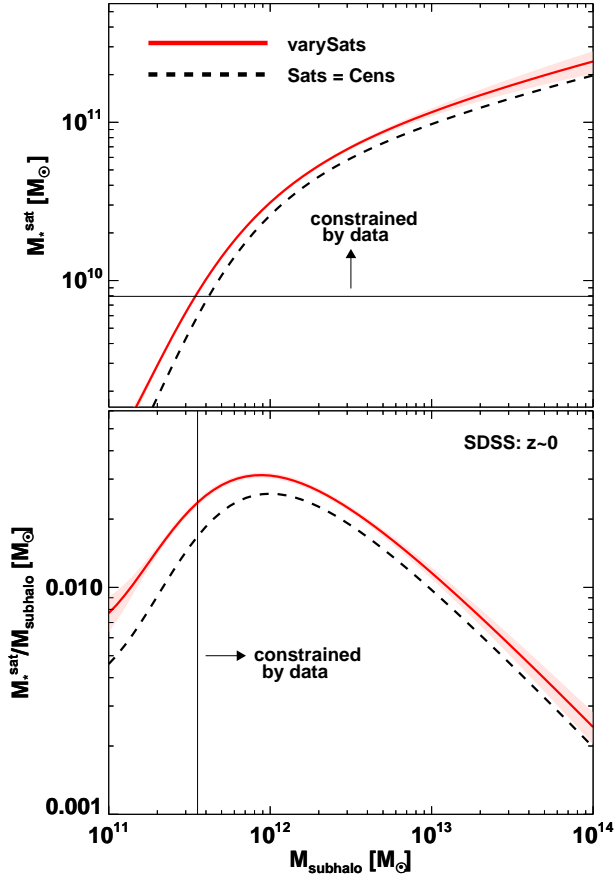


Figure 4. The satellite galaxy $M_* - M_h$ relation at $z \sim 0$. *Top panel:* The black curve represents the *Sats=Cens* model. The thin solid lines demarcate the mass range over which the model has been constrained by data. The red curve shows the best-fit relation for the *varySats* model. The lighter red band represents the 1σ uncertainty in the model. The *varySats* model is driven to higher masses in order to boost the clustering and satellite fractions. *Bottom panel:* Ratio between stellar mass and halo mass as a function of halo mass (the integrated star formation efficiency). The peak in star formation efficiency and the characteristic (sub)halo mass is nearly identical in both cases highlighting the mild stellar mass evolution in satellite galaxies and their similarity to the known lack of evolution of central galaxies.

eling of the 2PCF for the largest stellar mass threshold we consider, though our general results should hold. The bottom panel illustrates that the changes to the global GSMF of Baldry et al. (2008) (the same GSMF used in B12) implied by the *varySats* model are small and within the error bars.

To evaluate whether (and to what degree) the *varySats* model is preferred over the *Sats = Cens* model we employ the Aikake Information Criterion (AIC; see Liddle 2007 for details). AIC is preferred over a reduced χ^2 comparison since we do not take into account the covariance between f_{sat} and $w_p(r_p)$, which makes it difficult to discuss the goodness-of-fit in an absolute sense. Instead, using AIC we are able to comment on model preference. AIC is defined as $\text{AIC} = 2k + \chi^2_{\text{min}}$, where k is the number of free parameters in the model and in our case $\chi^2 = \chi^2(f_{\text{sat}}) + \chi^2(w_p(r_p))$. It is stressed in the literature to add a correction factor to AIC to take into account small sample size, such that $\text{AIC}_c =$

$\text{AIC} + 2k(k+1)/(N-k-1)$, where N is the number of data points ($N = 44$ for the $z \sim 0$ case). For the *Sats = Cens* model, $k = 0$, $\chi^2_{\text{Sats=Cens}} = 220.1$, the correction factor is 0, so $\text{AIC}_{c, \text{Sats=Cens}} = 220.1$. For the *varySats* model, $k = 7$, $\chi^2_{\text{varySats}} = 64.5$, the correction factor is 3.1, thus $\text{AIC}_{c, \text{varySats}} = 81.6$. When judged on Jeffreys scale for interpretation (Jeffreys 1961), the ΔAIC_c implies that the *varySats* model preference is considered ‘decisive’. Best-fit parameter values and the associated errors from our *varySats* model are listed in Table 1.

Turning to Figure 4, the top panel shows the satellite $M_* - M_h$ relation: satellite galaxy stellar mass vs. subhalo *peak* mass, M_{peak} . Again, the dashed black curve is the *Sats=Cens* model of B12, and the red curve shows the best-fit result from the *varySats* model. The solid red band shows the 1σ uncertainty in our *varySats* model. The *varySats* model implies that above the completeness limit of $\log(M^*) > 10.1 M_\odot$ of Reddick et al. (2012) there should be, on average, more stellar mass in satellite galaxies than the *Sats=Cens* model prediction by $\sim 10\%$ at all subhalo masses where the model can be constrained (although the two relations are consistent at the $2 - 3\sigma$ level for subhalo masses $\gtrsim 10^{13} h^{-1} M_\odot$). This implies that there will be more satellite galaxies in each SDSS stellar mass $w_p(r_p)$ threshold sample, which will boost the clustering and the satellite fractions.

The bottom panel shows the fraction of available baryons that have turned into stars (the integrated star formation efficiency) to illustrate at what subhalo mass galaxy formation is most efficient. Above the stellar mass limit where the model can be constrained, star formation in the *varySats* model has been slightly more efficient, on average, at all subhalo masses than central galaxies of the same mass. On the other hand, the characteristic mass for peak satellite galaxy star formation is approximately the same for central and satellite galaxies, though we urge caution with this conclusion as we are unable to probe the full range of the ‘turn over’ in the $M_* - M_h$ relation.

4.2. Clustering and the Satellite $M_* - M_h$ Relation at $z \sim 1$

As we turn to the $z \sim 1$ results, we find that the *Sats=Cens* model is in rather good agreement with the $z \sim 1$ DEEP2 data as shown in Figure 5. Again, the black dashed curve shows the *Sats=Cens* model prediction and the red curve is our best-fit *varySats* model. Measured satellite fractions were proved to be a powerful additional constraint at $z \sim 0$, however measurements are not available at $z \sim 1$. We find that c_0, c_1 , and c_6 are reasonably well constrained. However, c_2, c_3, c_4 , and c_5 are all unconstrained, thus parameter values (with errors) from our *varySats* model are not included in Table 1.

This is lack of constraining power is clearly manifested in Figure 6 where we show the best-fit $M_* - M_h$ relations. Here the errors on the satellite relation are significantly larger than at $z \sim 0$ (again, the light red band represents the 1σ uncertainty in the model), because the clustering data carry larger errors, only consider very large M_* thresholds, and because they are no measured satellite fractions to include in the fitting. In fact, we have found that the c_{0-6} parameter values corresponding to

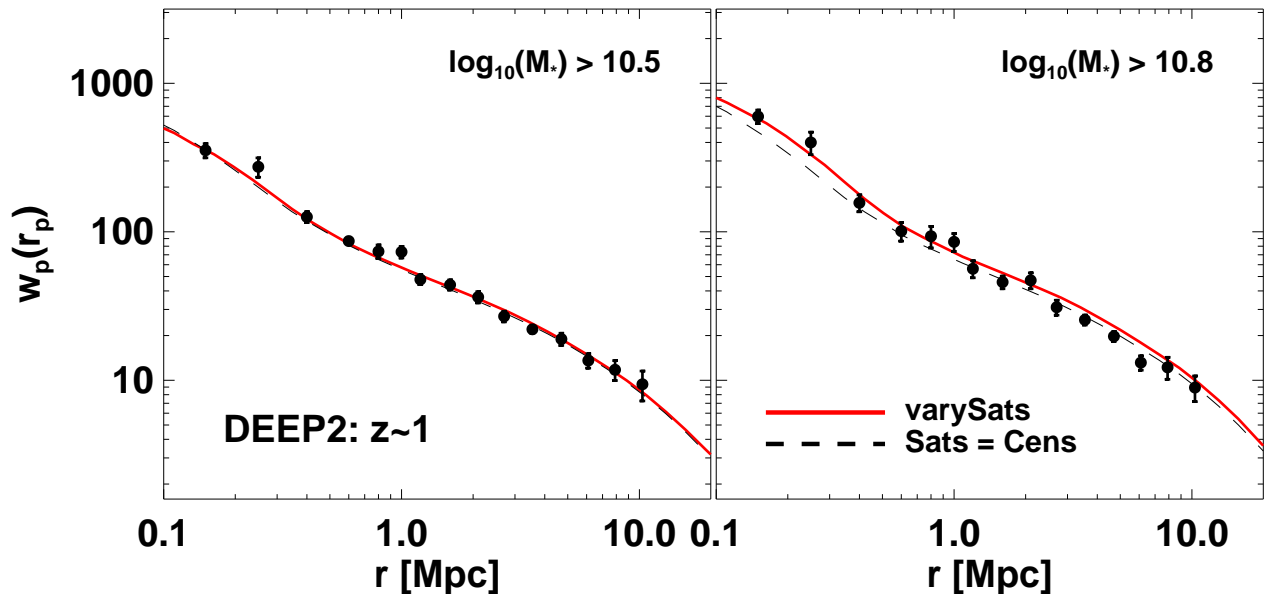


Figure 5. Same as Figure 2 but for $z \sim 1$ DEEP2 measurements of the projected correlation function of galaxies as a function of stellar mass from Mostek et al. (2012). Both models provide an excellent fit to the data.

the extrema of the 1σ error band in Figure 6 yield $w_p(r_p)$ predictions that are in good agreement with the data. They also appear to be reasonable when we test a much lower threshold for $w_p(r_p)$ of $\log(M_*) > 9.5$ where data are not available (i.e., there is a relative decrease in the overall amplitude of $w_p(r_p)$ as expected, yet no incongruous features). This reinforces the fact that it is not simply $w_p(r_p)$ measurements spanning a larger range in M_* thresholds that is necessary to constrain the satellite relation, rather the addition of measured satellite fractions as an additional, powerful constraint. Nonetheless, it is clear that the satellite relation is similar to the central relation at $z \sim 1$. Future data from larger area surveys at $z \sim 1$ should provide stronger constraints on the satellite $M_* - M_h$.

4.3. Clustering at $z \sim 2$

Wake et al. (2011) recently presented stellar-mass dependent angular correlation functions of galaxies at $z \sim 2$ based on the NMBS. The errors on the measurements are relatively large (compared to lower redshift) owing to the relatively small area of the NMBS fields. For this reason we did not attempt to fit the *VarySats* model to the data. Instead we simply compared the *Sats=Cens* model prediction to the existing clustering data. The result is shown in Figure 7. Again we emphasize that the *Sats=Cens* model makes a prediction for the clustering of galaxies, as this model was only tuned to fit the $z \sim 2$ GSMF. The model fits the data remarkably well over all scales and all mass ranges probed by the data. Future surveys covering a larger volume will be necessary to make more quantitative statements regarding the similarity of the satellite and central $M_* - M_h$ relations.

4.4. Satellite Fractions at $z \sim 0, 1$ and 2

Our modeling describes how galaxy stellar mass should be mapped to host halos and subhalos. This mapping can be used to infer satellite fractions as a function of stellar mass and redshift. Figure 8 shows the satellite fraction where constraining data exists as a function of galaxy stellar mass from our best-fit *varySats* model at $z \sim 0$ and 1 (red and blue curves). The green curve is the *Sats=Cens* model at $z \sim 2$. The solid bands are the associated 1σ errors. The *varySats* model was not considered at $z \sim 2$, thus no errors are shown for this curve. Satellite fractions decline with increasing redshift in agreement with previous studies (Zentner et al. 2005; Zheng et al. 2007; Wetzel & White 2010; Watson et al. 2011).

5. DISCUSSION

5.1. Implications for Satellite Galaxy Evolution

The primary result of this paper is that the mean relation between galaxy stellar mass and halo mass is similar for central and satellite galaxies since at least $z \sim 2$. We are able to put strong constraints on the satellite $M_* - M_h$ relation at $z \sim 0$, and we find that there is a slight difference in the sense that satellites appear to have somewhat higher stellar masses at fixed halo mass. At $z \sim 1$ and 2 the satellite $M_* - M_h$ relation is consistent with the central relation, but there is still considerable room for differences between the two relations due to the lack of measured satellite fractions and large errors on the clustering data. In this section we explore the implications of these results for the evolution of satellite galaxies.

There is an emerging consensus that the global $M_* - M_h$ relation evolves little if at all since $z \sim 2$ (e.g., Yang et al. 2012; Moster et al. 2013; Behroozi et al. 2012b; Wang et al. 2012; Leauthaud et al. 2012). As discussed in previous sections, the satellite fraction in mass-

Table 1
BEST-FIT PARAMETERS FOR THE *varySats* MODEL

redshift	c_0	c_1	c_2	c_3	c_4	c_5	c_6
$z = 0$	$1.024^{+0.011}_{-0.058}$	$0.957^{+0.001}_{-0.009}$	$0.992^{+0.001}_{-0.002}$	$0.732^{+0.156}_{-0.0145}$	$1.029^{+0.092}_{-0.036}$	$0.986^{+0.067}_{-0.192}$	$0.834^{+0.060}_{-0.074}$

Note. — Best-fit parameter values from our *varySats* model at $z = 0$. The errors on the parameter values represent the extrema of the middle 68.3% of our MCMC chains after sorting by χ^2 . The *varySats* model at $z \sim 1$ could not be constrained, hence no results are shown at that redshift. Due to the large errors on the data at $z \sim 2$ we do not attempt to constrain the *varySats* model.

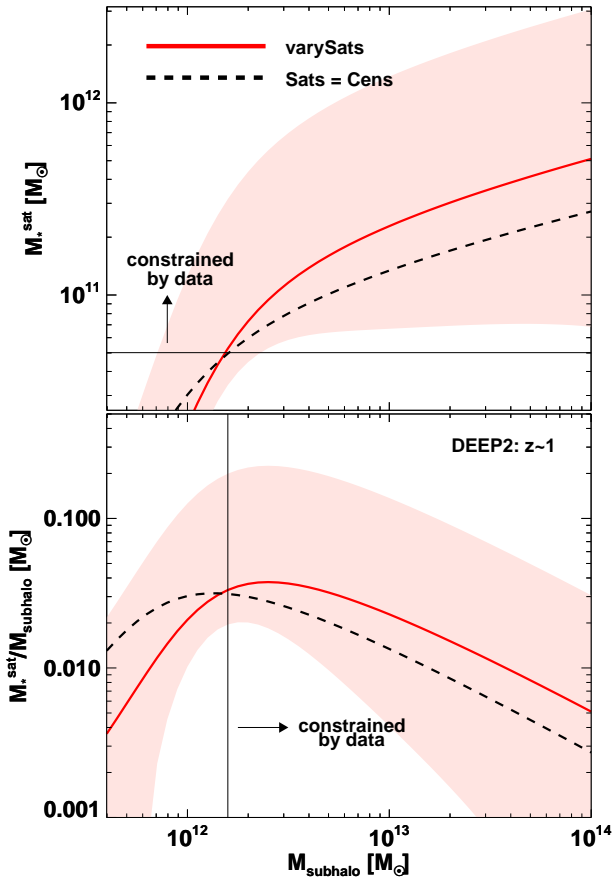


Figure 6. Same as Figure 4 but for $z \sim 1$. The errors on the $z \sim 1$ *varySats* model are considerably larger than at $z \sim 0$, with the result that the $M_* - M_h$ relation for this model is consistent with the relation for the simple *Sats=Cens* model.

limited samples is always $\lesssim 30\%$ and decreases with increasing redshift. The global relation is therefore, to a good approximation, the central galaxy relation. The weakly evolving $M_* - M_h$ relation for central galaxies is one of the main facts that explains the lack of evolution in the satellite galaxy $M_* - M_h$ relation. In the discussion that follows we will assume for simplicity that the central relation is constant in time.

First, it is worth briefly considering scenarios that are inconsistent with our results. Satellite galaxies, on average, cannot have experienced large (order unity) growth in stellar mass since their accretion, nor can they have experienced a large loss in mass (unless they are altogether destroyed). These possibilities would result in satellite $M_* - M_h$ relations significantly offset from the central

galaxy relation. Of course, since the resulting satellite relation is an integral over the past history of the satellite, in principle our results allow for a scenario in which the average satellite has *both* gained substantial mass via e.g., star formation *and* lost substantial mass via e.g., tidal stripping. This seems implausible, at least for the average satellite. It is therefore clear that any successful scenario must allow for only modest growth in the stellar mass of satellite galaxies while they are satellites.

In another scenario for satellite galaxy evolution, stellar mass growth is immediately halted when a galaxy becomes a satellite. In this case the satellite $M_* - M_h$ relation would then be identical to the unevolving central relation. This would be so because for any scenario the subhalo peak mass, M_{peak} , does not evolve after accretion by definition, and in this scenario neither does M^* . Such a possibility is reminiscent of previous generations of semi-analytic models. This is because in such models it was assumed that, upon infall, a satellite galaxy will be instantaneously stripped of its hot gas atmosphere. Consequently, it experiences quenching after a cold gas consumption time (which typically is very short) and little M_* growth could occur. However, these earlier models have been shown to overproduce the fraction of quiescent satellites as a function of mass (e.g., Weinmann et al. 2006; Font et al. 2008).

We now turn to a more plausible scenario for satellite galaxy evolution. In this scenario, all satellites continue to grow in stellar mass as if they were still central galaxies for a significant fraction of their lifetime (see also Wetzel et al. 2012b). If we adopt the relation between star formation rate (SFR) and stellar mass measured in the local universe by Salim et al. (2007) along with a typical time since accretion for satellites of 4 Gyr (see e.g., Zentner et al. 2005; Wetzel et al. 2012b), then the average galaxy with $M^* \sim 10^{11} M_\odot$ will have increased its mass by $\sim 10\%$ since becoming a satellite, as a result of its star formation continuing as if it were a central galaxy. Owing to the fact that the SFR/M^* relation is so shallow, the fraction of mass grown is a weak function of mass. Thus, in this scenario, the satellite $M_* - M_h$ relation would be shifted approximately 10% higher compared to the central relation (i.e., at fixed halo mass satellites would have $\sim 10\%$ more stellar mass). It is interesting that this shift is similar to what we find herein at $z \sim 0$. Given the systematic uncertainties that exist at the 10% level in these relations we caution against overinterpreting this similarity, although we will now briefly explore why satellites may evolve like centrals for most of their evolution.

Satellite galaxies can be subject to numerous physical processes capable of altering their evolution. This has been well-documented in very dense environments,

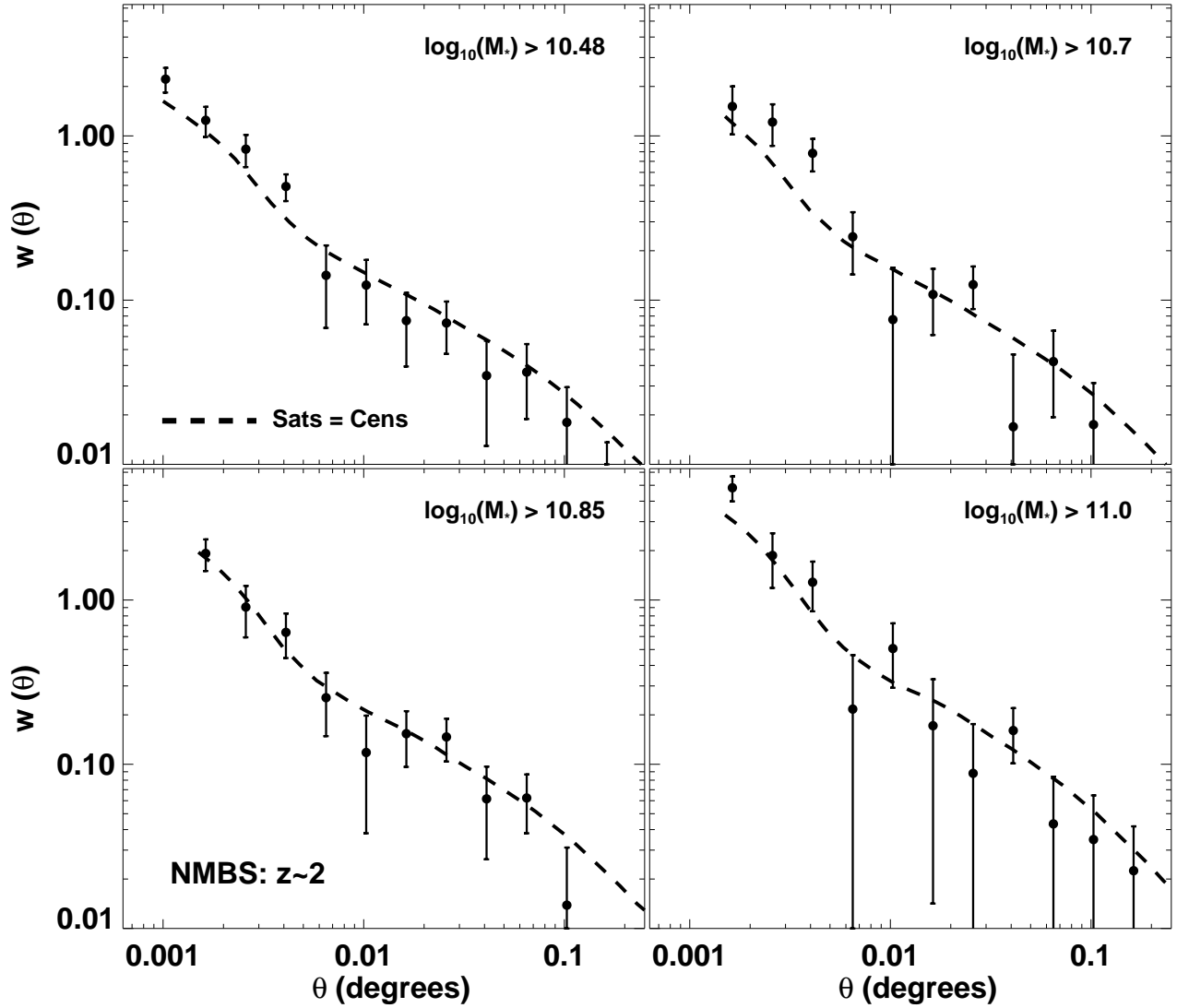


Figure 7. Same as Figures 2 and 5 but for $z \sim 2$ NMBS measurements of the angular correlation function of galaxies as a function of stellar mass from Wake et al. (2011). The *Sats=Cens* model is in remarkably good agreement with the data. Due to the relatively large error bars on the data the *varySats* model is unconstrained and so is not included in the figure.

such as large galaxy groups and clusters. For instance, ram pressure stripping can reduce the gas supply, stifling star formation. However, these processes are less effective in modest-sized groups where most satellites reside. In a given mass-limited sample of galaxies, most satellites are found in relatively quiescent environments, e.g., in a halo that contains one central and one satellite galaxy. This is evident in the group multiplicity function (Berlind et al. 2006; Hearin et al. 2012) and in halo occupation models (Zehavi et al. 2005; van den Bosch et al. 2007; Zehavi et al. 2011). Thus, for the typical satellite, physical processes capable of altering its evolution are relatively inefficient.

Perhaps more importantly, dynamical friction timescales at the group scale are shorter than at the cluster scale (for a satellite of the same mass), meaning that satellite galaxies in groups spiral toward the center and merge with the central galaxy more quickly than in

rich clusters. This implies that there is a relatively small amount of time for the group environment to shape the physical properties of a satellite before that satellite is destroyed and/or merges with the central object. This effect becomes even stronger at higher redshifts because dynamical times are shorter (although this effect may be mitigated to some extent due to the fact the SFRs are higher at higher redshift). This also partly explains the lower satellite fractions at higher redshifts discussed in Section 4.4. However, we caution that in this work we are mainly considering massive satellites. The situation at lower masses is unconstrained in the present work (see Pasquali et al. 2010).

This picture was motivated in part by the recent results of Wetzel et al. (2012b), who analyzed the properties of low redshift satellite and central galaxies including stellar masses and star formation rates. These authors concluded that, after it is accreted, the typical satellite

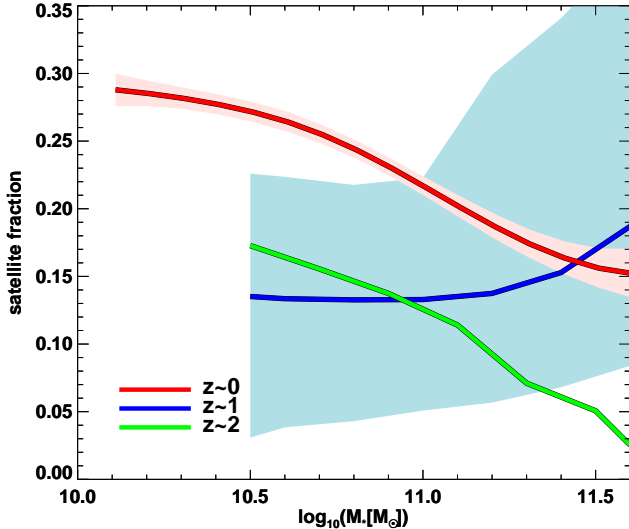


Figure 8. Satellite fraction as a function of galaxy stellar mass in bins of $\Delta\log(M^*) = 0.1$ as inferred from our best-fit *varySats* model at $z \sim 0$ and 1 and from the *Sats=Cens* model at $z \sim 2$. Satellite fractions are only plotted over the mass range where there is constraining data.

continues to form stars as if it were still a central galaxy for 2–4 Gyr before star formation is quenched. This conclusion follows naturally from the fact that there exists a strong bimodality in satellite galaxy SFRs combined with the fact that the locations of the two peaks are similar to those of central galaxies with the same stellar mass (Wetzel et al. 2012a).

The similarity between satellite and central $M_* - M_h$ relations thus appears to be a natural outcome of several facts: 1) the weakly or unevolving $M_* - M_h$ relation for central galaxies; 2) the hierarchical growth of structure, which ensures that the majority of satellite galaxies (at least with $M^* > 10^{10} M_\odot$) are not strongly affected by their environments for most of their relatively short lives; 3) typical SFRs at late times are low, resulting in long mass doubling times; and 4) the combination of the relatively short satellite lifetimes and long mass doubling times suggests that the typical satellite will not have grown substantially in mass since the time it became a satellite, and therefore the satellite relation will not differ significantly from the central galaxy relation when the satellite was accreted, which in turn differs little from the present day central relation.

5.2. Comparison to Previous Work

There have been several previous studies that attempted to separately constrain the satellite and central galaxy $M_* - M_h$ relations. Wang et al. (2006) were the first to consider such a distinction. They adopted a method that used galaxy positions and velocities determined from the orbital and merging histories of halos and subhalos from a full cosmological simulation (as opposed to a statistical HOD approach) to predict observed galaxy statistics. Galaxy properties such as luminosity and stellar mass were parameterized as a function of M_{acc} , where the functional forms of the $L - M_h$ and $M^* - M_h$ relations were adopted from a semi-analytic model as reference. They were able to success-

fully model the observed stellar mass/luminosity functions and 2PCFs at low redshift and found central and satellite $M^* - M_h$ relations that were identical within the errors. These results are broadly consistent with our work, although recent high-precision measurements of $w_p(r_p)$ and f_{sat} argue for a slight difference between the central and satellite $M_* - M_h$ relations.

Both Yang et al. (2012) and Moster et al. (2013) treat satellite galaxies ‘self-consistently’, wherein the $M_* - M_h$ relation for satellites is used at the epoch of accretion (for instance, see the multi-epoch abundance matching technique described in Moster et al. 2013). Both of these studies find that the the global $M_* - M_h$ relation evolves with redshift (albeit weakly), thus it is also inferred that at the $z \sim 0$ central and satellite relations are different.

Rodríguez-Puebla et al. (2012) also considered distinct $M_* - M_h$ relations for centrals and satellites in an abundance matching context. They used the $z \sim 0$ GSMF decomposed into central and satellite galaxies and used abundance matching separately for the centrals and satellites. They found models based on M_{acc} were in agreement with measured conditional stellar mass functions and correlation functions only when the satellite $M_* - M_h$ relation was slightly different from the central relation (by $\lesssim 0.1$ dex at $M > 10^{12} M_\odot$), a result in general accord with our low- z findings.

Neistein & Khochfar (2012) used abundance matching within a full cosmological simulation to further investigate the $M_* - M_h$ connection. Motivated by Neistein et al. (2011a), satellite stellar mass depended on both M_{acc} and the host halo mass at $z = 0$, and the satellite $M_* - M_h$ relation was allowed to differ from the central relation. The authors considered the abundance of galaxies, the 2PCF and weak lensing measurements in their modeling and they found that the $M_* - M_h$ relation for satellites at $z = 0$ was poorly constrained, such that a wide range of relations were consistent with the data, resulting in satellite fractions spanning $f_{\text{sat}} = 0.05 - 0.8$. This result suggested that the inclusion of the measured satellite fraction as an additional statistic could be key to further constraining the satellite $M_* - M_h$ relation.

Each of these studies attempted to separately constrain the satellite and central galaxy $M_* - M_h$ relations at low redshift, allowing us to piece together a clearer picture of the two relations. While there are several differences in the methodology between our work and the aforementioned studies, the principal distinction is our use of the measured satellite fractions from Reddick et al. (2012) as an additional model constraint. The power of using satellite fractions to constrain the satellite $M_* - M_h$ relation can also be seen in our Figure 1. However, at $z \sim 1$ satellite fractions are not available, and our derived satellite $M_* - M_h$ relation is consequently more uncertain. In fact, the uncertainties we derive are qualitatively consistent with the error envelope quoted by Neistein & Khochfar (2012) based on their analysis of $z \sim 0$ data, also without satellite fractions. Additionally, one can see from Figure 3 of Wang et al. (2012) that the successful modeling of 2PCFs from Wang et al. (2006) over-predicts satellite fractions from the group catalogs of Yang et al. (2008). Our results argue that the observed 2PCF and GSMF are not enough to provide strong constraints on the satellite $M_* - M_h$ relation. However, estimates of the mass-dependent satellite fraction, in conjunction with these

other statistics, result in much smaller errors on the inferred satellite $M_* - M_h$ relation.

It is also important to emphasize here that we do not allow freedom in the central relation in order to limit computation time. We argue that this approximation is justified because the global GSMF and 2PCFs on large scales (where central galaxies dominate) are well-fit by our model. However, incorporating a parameterized $M_* - M_h$ central relation may result in a larger range of possible models for the satellites. We leave this possibility for future work.

Finally, Reddick et al. (2012) showed that v_{peak} , the maximum circular velocity analog to M_{peak} , was the best halo property for matching low- z clustering data. We have adopted the latter herein in order to exploit the newly calibrated $M_* - M_h$ from B12, which was derived for masses rather than circular velocities. It remains an open question if the satellite and central relations would be even more similar if circular velocities were used in place of halo masses.

6. SUMMARY

In this paper we have explored the relation between satellite galaxies and their dark matter halos since $z \sim 2$. We take advantage of precision measurements of the galaxy 2PCF, a statistic which is highly sensitive to the *satellite* galaxy population. Previous studies have used low- and intermediate-redshift clustering measurements (see Moster et al. 2010; Yang et al. 2012) as the 2PCF provides a powerful constraint to better understand the evolution of stellar mass in satellite galaxies. For the first time we have incorporated clustering measurements as a function of stellar mass out to high redshift, allowing us to model the evolution of satellite galaxies over ~ 10 Gyr of cosmic time.

To model the satellite galaxies, we started by adopting the $M_* - M_h$ relation of B12 which was shown to accurately reproduce GSMFs out to $z \sim 8$. We applied this relation to halos and subhalos in the Bolshoi dissipationless N -body simulation identified by the ROCKSTAR halo finder at $z \sim 0, 1$ and 2. We then calculated the projected 2PCFs to compare to observations at $z \sim 0$ and 1 as well as angular correlation functions at $z \sim 2$. This approach was named the *Sats=Cens* model as the B12 $M_* - M_h$ relation gives the same functional form for both central and satellite galaxies. The *Sats=Cens* model was shown to slightly under-predict satellite fractions and clustering measurements in low-mass galaxies at low redshift. This prompted us to introduce a model that allowed for more flexibility in the satellite $M_* - M_h$ relation, the *varySats* model. We retained the B12 best-fit relation for centrals and fit for the satellite relation, using an MCMC method to probe parameter space. Our technique is essentially a hybrid between the halo occupation distribution and abundance matching methods, in the sense that we adopt the abundance matching requirement that satellites reside within subhalos while allowing for a flexibility in the galaxy-halo relation common to halo occupation models. Our modeling approach yields the following principal results.

- The clustering and satellite fraction data at $z \sim 0$ imply that the satellite galaxy $M_* - M_h$ relation is nearly identical to the central galaxy relation, with

a preference for the stellar mass of satellites to be $\sim 10\%$ larger than centrals at fixed halo mass (the two relations are consistent at $2-3\sigma$ for subhalo masses $\gtrsim 10^{13} M_\odot$). At $z \sim 1$ the satellite and central $M_* - M_h$ relations are indistinguishable within the (considerable) errors.

- Our models provide an excellent fit to the stellar-mass dependent clustering of galaxies at $z \sim 1$. This stands in contrast to several previous studies that were unable to reproduce the observed $z \sim 1$ B -band luminosity-dependent clustering through abundance matching (Wetzel & White 2010; Gerke et al. 2012). The success herein may perhaps be due to the fact that stellar mass is more strongly correlated with dark matter halo mass than B -band luminosity.
- At $z \sim 2$, we find that a simple model in which the satellite $M_* - M_h$ relation is the same as the central relation is in good agreement with two-point clustering data at all scales and all stellar masses. However, at present the errors on the data are too large to constrain the more flexible satellite model.

While the detailed physics of galaxy formation is complex and highly nonlinear, our results add to the emerging consensus that the basic properties of galaxies are surprisingly regular and simply connected to the underlying dark matter distribution. The $M_* - M_h$ relation for central galaxies has been shown to evolve little since $z \sim 4$ (Yang et al. 2012; Moster et al. 2013; Behroozi et al. 2012b). Along with this lack of evolution, Behroozi et al. (2012a) showed that there exists a nearly constant peak in star formation efficiency in halos with characteristic mass $10^{11.7}$ since $z \sim 4$, consistent with theoretical predictions of the halo mass scale for the shock heating of accreted gas (Rees & Ostriker 1977; White & Rees 1978; Blumenthal et al. 1984; Kereš et al. 2005; Dekel & Birnboim 2006). Additionally, this is also the mass scale when effects due to AGN feedback become significant, which can have a dramatic effect on star formation (Teyssier et al. 2011; Martizzi et al. 2012). These results for central galaxies also appear to hold for the satellites. The reason for this is not yet entirely clear, but it is likely related to the fact that the typical $\sim L^*$ satellite galaxy resides in a poor group where transformation processes are weak and lifetimes are short.

This material is based upon work supported by the National Science Foundation under Award No. AST-1202698. We would like to thank the referee for a careful and highly constructive referee report. We would also like to thank Andreas Berlind, Andrew Wetzel, Martin White, Rachel Reddick, and Risa Wechsler for insightful discussions and Joanne Cohn, Peter Behroozi, Andrey Kravtsov and Andrew Hearin for helpful comments on an earlier draft. Finally, DFW and CC would also like to thank Rachel Reddick, Nick Mostek and David Wake for providing their data in electronic format and Peter Behroozi for access to the Bolshoi halo catalogs.

- Abazajian, K. N., et al. 2009, *ApJS*, 182, 543
- Baldry, I. K., Glazebrook, K., & Driver, S. P. 2008, *MNRAS*, 388, 945
- Behroozi, P. S., Wechsler, R. H., & Conroy, C. 2012a, *ArXiv*: 1209.3013
- . 2012b, *ArXiv*: 1207.6105
- Behroozi, P. S., Wechsler, R. H., & Wu, H.-Y. 2011a, *ArXiv*: 1110.4372
- Behroozi, P. S., Wechsler, R. H., Wu, H.-Y., Busha, M. T., Klypin, A. A., & Primack, J. R. 2011b, *ArXiv*: 1110.4370
- Berlind, A. A., et al. 2006, *ApJS*, 167, 1
- Berlind, A. A., & Weinberg, D. H. 2002, *ApJ*, 575, 587
- Berrier, J. C., Bullock, J. S., Barton, E. J., Guenther, H. D., Zentner, A. R., & Wechsler, R. H. 2006, *ApJ*, 652, 56
- Berrier, J. C., & Cooke, J. 2012, *MNRAS*, 426, 1647
- Blanton, M. R., et al. 2005, *AJ*, 129, 2562
- Blumenthal, G. R., Faber, S. M., Primack, J. R., & Rees, M. J. 1984, *Nature*, 311, 517
- Bryan, G. L., & Norman, M. L. 1998, *ApJ*, 495, 80
- Chabrier, G. 2003, *PASP*, 115, 763
- Conroy, C., & Wechsler, R. H. 2009, *ApJ*, 696, 620
- Conroy, C., Wechsler, R. H., & Kravtsov, A. V. 2006, *ApJ*, 647, 201
- Cooray, A., & Sheth, R. 2002, *Phys. Rep.*, 372, 1
- Dekel, A., & Birnboim, Y. 2006, *MNRAS*, 368, 2
- Dunkley, J., Bucher, M., Ferreira, P. G., Moodley, K., & Skordis, C. 2005, *MNRAS*, 356, 925
- Font, A. S., et al. 2008, *MNRAS*, 389, 1619
- Gerke, B. F., Wechsler, R. H., Behroozi, P. S., Cooper, M. C., Yan, R., & Coil, A. L. 2012, *ArXiv*: 1207.2214
- Gunn, J. E., & Gott, III, J. R. 1972, *ApJ*, 176, 1
- Guo, Q., White, S., Li, C., & Boylan-Kolchin, M. 2010, *MNRAS*, 404, 1111
- Hearin, A. P., Zentner, A. R., Berlind, A. A., & Newman, J. A. 2012, *ArXiv*: 1210.4927
- Jeffreys, H. 1961, *Theory of Probability*, 3rd ed., Oxford University Press
- Kereš, D., Katz, N., Weinberg, D. H., & Davé, R. 2005, *MNRAS*, 363, 2
- Klypin, A. A., Trujillo-Gomez, S., & Primack, J. 2011, *ApJ*, 740, 102
- Kravtsov, A. V., Berlind, A. A., Wechsler, R. H., Klypin, A. A., Gottlöber, S., Allgood, B., & Primack, J. R. 2004a, *ApJ*, 609, 35
- Kravtsov, A. V., Gnedin, O. Y., & Klypin, A. A. 2004b, *ApJ*, 609, 482
- Kravtsov, A. V., & Klypin, A. A. 1999, *ApJ*, 520, 437
- Kravtsov, A. V., Klypin, A. A., & Khokhlov, A. M. 1997, *ApJS*, 111, 73
- Larson, R. B., Tinsley, B. M., & Caldwell, C. N. 1980, *ApJ*, 237, 692
- Leauthaud, A., et al. 2012, *ApJ*, 744, 159
- Leitner, S. N. 2012, *ApJ*, 745, 149
- Liddle, A. R. 2007, *MNRAS*, 377, L74
- Martizzi, D., Teyssier, R., & Moore, B. 2012, *MNRAS*, 420, 2859
- Moore, B., Lake, G., & Katz, N. 1998, *ApJ*, 495, 139
- Mostek, N., Coil, A. L., Cooper, M. C., Davis, M., Newman, J. A., & Weiner, B. 2012, *ArXiv*: 1210.6694
- Moster, B. P., Naab, T., & White, S. D. M. 2013, *MNRAS*, 428, 3121
- Moster, B. P., Somerville, R. S., Maulbetsch, C., van den Bosch, F. C., Macciò, A. V., Naab, T., & Oser, L. 2010, *ApJ*, 710, 903
- Nagai, D., & Kravtsov, A. V. 2005, *ApJ*, 618, 557
- Neistein, E., & Khochfar, S. 2012, *ArXiv*: 1209.0463
- Neistein, E., Li, C., Khochfar, S., Weinmann, S. M., Shankar, F., & Boylan-Kolchin, M. 2011a, *MNRAS*, 416, 1486
- Neistein, E., Weinmann, S. M., Li, C., & Boylan-Kolchin, M. 2011b, *MNRAS*, 414, 1405
- Newman, J. A., et al. 2012, *ArXiv*: 1203.3192
- Padmanabhan, N., et al. 2008, *ApJ*, 674, 1217
- Pasquali, A., Gallazzi, A., Fontanot, F., van den Bosch, F. C., De Lucia, G., Mo, H. J., & Yang, X. 2010, *MNRAS*, 407, 937
- Peacock, J. A., & Smith, R. E. 2000, *MNRAS*, 318, 1144
- Purcell, C. W., Bullock, J. S., & Zentner, A. R. 2007, *ApJ*, 666, 20
- Reddick, R. M., Wechsler, R. H., Tinker, J. L., & Behroozi, P. S. 2012, *ArXiv*: 1207.2160
- Rees, M. J., & Ostriker, J. P. 1977, *MNRAS*, 179, 541
- Rodríguez-Puebla, A., Drory, N., & Avila-Reese, V. 2012, *ApJ*, 756, 2
- Salim, S., et al. 2007, *ApJS*, 173, 267
- Scoccimarro, R., Sheth, R. K., Hui, L., & Jain, B. 2001, *ApJ*, 546, 20
- Seljak, U. 2000, *MNRAS*, 318, 203
- Simha, V., Weinberg, D., Dave, R., Fardal, M., Katz, N., & Oppenheimer, B. D. 2010, *ArXiv*: 1011.4964
- Tasitsiomi, A., Kravtsov, A. V., Wechsler, R. H., & Primack, J. R. 2004, *ApJ*, 614, 533
- Teyssier, R., Moore, B., Martizzi, D., Dubois, Y., & Mayer, L. 2011, *MNRAS*, 414, 195
- Tinker, J., Wetzel, A., & Conroy, C. 2013, *ArXiv*: 1107.5046
- Vale, A., & Ostriker, J. P. 2004, *MNRAS*, 353, 189
- . 2006, *MNRAS*, 371, 1173
- van den Bosch, F. C., et al. 2007, *MNRAS*, 376, 841
- van Dokkum, P. G., et al. 2009, *PASP*, 121, 2
- Wake, D. A., et al. 2011, *ApJ*, 728, 46
- Wang, L., et al. 2012, *ArXiv*: 1203.5828
- Wang, L., & Jing, Y. P. 2010, *MNRAS*, 402, 1796
- Wang, L., Li, C., Kauffmann, G., & De Lucia, G. 2006, *MNRAS*, 371, 537
- Watson, D. F., Berlind, A. A., & Zentner, A. R. 2011, *ApJ*, 738, 22
- . 2012, *ApJ*, 754, 90
- Weinmann, S. M., van den Bosch, F. C., Yang, X., Mo, H. J., Croton, D. J., & Moore, B. 2006, *MNRAS*, 372, 1161
- Wetzel, A. R., Tinker, J. L., & Conroy, C. 2012a, *MNRAS*, 424, 232
- Wetzel, A. R., Tinker, J. L., Conroy, C., & van den Bosch, F. C. 2012b, *ArXiv*: 1206.3571
- Wetzel, A. R., & White, M. 2010, *MNRAS*, 403, 1072
- White, M., Zheng, Z., Brown, M. J. I., Dey, A., & Jannuzi, B. T. 2007, *ApJ*, 655, L69
- White, S. D. M., & Rees, M. J. 1978, *MNRAS*, 183, 341
- Yang, X., Mo, H. J., & van den Bosch, F. C. 2003, *MNRAS*, 339, 1057
- . 2008, *ApJ*, 676, 248
- . 2009, *ApJ*, 695, 900
- Yang, X., Mo, H. J., van den Bosch, F. C., Zhang, Y., & Han, J. 2012, *ApJ*, 752, 41
- Zehavi, I., et al. 2011, *ApJ*, 736, 59
- . 2005, *ApJ*, 630, 1
- Zentner, A. R., Berlind, A. A., Bullock, J. S., Kravtsov, A. V., & Wechsler, R. H. 2005, *ApJ*, 624, 505
- Zheng, Z., et al. 2005, *ApJ*, 633, 791
- Zheng, Z., Coil, A. L., & Zehavi, I. 2007, *ApJ*, 667, 760